Performance Analysis of an Improved 3-D PET Monte Carlo Simulation and Scatter Correction

C. H. Holdsworth, *Student Member, IEEE*, C. S. Levin, *Member, IEEE*, M. Janecek, *Student Member, IEEE*, M. Dahlbom, *Senior Member, IEEE*, and E. J. Hoffman, *Fellow, IEEE*

***Abstract*—We are developing an accelerated Monte Carlo simulation of positron emission tomography (PET) that can be used for scatter correction of three-dimensional (3-D) PET data. Our Monte Carlo technique accurately accounts for single, multiple, and dual Compton scatter events, attenuation through the patient bed, and activity from outside the field of view. We have incorporated innovative sampling techniques that are compatible with our simulation approach, increasing computational efficiency by a factor of seven while improving accuracy through more sophisticated stratification and by incorporating the true energy response of the scanner. The required execution time to acquire 10 million scatter coincidence events for a 3-D thorax PET scan is only 4 min on a 300-MHz Sun dual-processor workstation. We demonstrate that for a low-noise thorax phantom study, image data corrected using the Monte Carlo 3-D PET scatter correction demonstrate no statistically significant deviation from the true activity concentration provided corresponding input data are accurate. The speed and accuracy of our simulation makes it an efficient research tool for studying scatter effects in PET and a practical scatter correction for 3-D PET clinical imaging.**

***Index Terms*—Compton scatter, Monte Carlo simulation, photon tracking, positron emission tomography (PET), sampling techniques, scatter correction, three-dimensional (3-D) PET, variance reduction.**

I. Introduction

DETECTED scatter coincidence events degrade image contrast and compromise quantitative accuracy in positron emission tomography (PET). Scatter effects become a significant problem especially in three-dimensional (3-D) PET when the lead septa are removed to achieve a five-fold increase in sensitivity. The scatter fraction for whole-body 3-D PET studies increases from 10–20% in two-dimensional (2-D) PET to 40–60% in 3-D PET [1]. Scatter correction for the resulting images is a challenging problem. Analytical calculation and correction of the scatter distribution acquired from a PET scan is difficult, particularly for the multiple or dual scatter distribution [2].

Monte Carlo computer simulations use the known initial conditions and physics of a system to generate data using random numbers to determine probabilistic behavior. The accuracy of the simulated data is limited only by the accuracy of the input data and the detail of the model employed in the simulation. This technique can be used to solve complex problems that are impossible to solve analytically.

Although other Monte Carlo simulations for PET [3]–[6] do use techniques to reduce computation times, these programs are not designed primarily for speed. Typical execution rates of a simulated 3-D PET thorax acquisition are on the order of 2–5 ms per acquired event on a 300-MHz Sun dual-processor workstation [7], [8]. At this acquisition rate, it would take almost a day to simulate the equivalent of 10 million equally weighted scatter coincidence events.

Our accelerated Monte Carlo code simulates 10 million equally weighted scatter coincidence events in only 4 min on a 300-MHz Sun dual processor workstation. The short execution time makes this simulation an effective tool for detailed investigation of the effect of scatter in PET imaging. The accelerated Monte Carlo simulation is now fast enough to implement as a scatter correction for clinical patient data as well as for microPET studies.

The Monte Carlo method of 3-D PET scatter correction is dependent on activity distribution and attenuation media. To perform a Monte Carlo calculated scatter correction for a 3-D PET scan, the emission image volume is first reconstructed to generate the relative activity distribution that determines the number of annihilations to simulate in each voxel. The transmission data are reconstructed to create the voxelized attenuation map that helps determine the interactions of individual simulated photons. The Monte Carlo code uses these data to generate a scatter distribution that can be scaled and then subtracted from the original normalized sinogram prior to a second image reconstruction. The Monte Carlo scatter correction has the potential for greater accuracy than any other method currently employed [3].

II. Materials and Methods

A. Simulation

Our simulation code was originally written in C-Language [9], [10]. In previous work, we streamlined the program, implemented some simple variance reduction techniques, and improved the efficiency by a factor of 24 while improving the accuracy of the program [11]. For this paper, we introduce innovative variance-reduction techniques and improved the efficiency of the program by an additional factor of seven. The simulation now incorporates accurate energy response and improved stratification. Simulations were performed on a dual 300-MHz processor Sun Ultra II Creator workstation. Although the data presented in this paper are primarily the result of simulations

Manuscript received April 5, 2001; revised July 17, 2001. This work was supported in part by NCI under Grant R01-CA56655 and by the U.S. Department of Energy under Contract DEF G0387-ER6061.

C. H. Holdsworth, M. Janecek, M. Dahlbom, and E. J. Hoffman are with the UCLA School of Medicine, Los Angeles, CA 90095 USA (e-mail: choldsworth@mednet.ucla.edu).

C. S. Levin is with the UCLA School of Medicine, Los Angeles, CA 90095 USA, the UCSD School of Medicine, San Diego, CA 92161 USA, and the San Diego VA Medical Center, San Diego, CA 92161 USA.

Publisher Item Identifier S 0018-9499(02)01643-X.

of the Siemens/CTI ECAT EXACT HR+ 962 PET system, our Monte Carlo code can be easily modified to simulate any ring geometry. To demonstrate this, we have included data from a simulation of a microPET scan.

We currently use the system's simulation-based scatter correction [12] during reconstruction of the emission image volume to provide a more accurate initial activity distribution estimate for the simulation. Once the required data are read into memory, the relative number of annihilations to be simulated in each voxel is determined by the emission image. Annihilations are not simulated in air voxels.

The transmission image determines the attenuation coefficient in each voxel. As expected, the simulation is sensitive to noise and inaccuracy in the voxelized attenuation map. Currently, median smoothing, thresholding, and an essentially noiseless attenuation map of the bed are used to reduce the effects of noise while retaining adequate resolution for edge detection. We have seen that noise and error in the input images, particularly in the attenuation image, will result in error in simulation sinograms and images.

Annihilation photons are transported through the medium using the very efficient delta scattering method [13], which is accurate to within 0.07% [11]. The simulated photons are propagated through the attenuation map using random numbers to determine locations and results of interactions. If a Compton scatter event occurs, the new direction and energy of the scattered photon are determined using tabulated values derived from a product of the actual energy response of the scanner [14] and data generated by the Klein–Nishina formula (see Section III-B). Once a photon escapes the body, it is transported to the detector gantry. If both photons from an annihilation are detected, a coincidence event is recorded. The event is considered "scatter" if either of the detected photons encountered a Compton scatter interaction, and a "primary" event otherwise. After all annihilations in every voxel of the input activity distribution have been simulated, the program writes the scatter and primary sinograms to a file.

To employ a scatter correction, a global scale factor is determined by matching the simulated total distribution (sum of primary and scatter) to the original normalized measured sinogram. This scale factor is used to properly scale the simulated scatter distribution that is subtracted from the measured sinogram prior to reconstruction. To reduce the scatter correction's sensitivity to error and noise in the input images, we are investigating using different scale factors for different regions of the sinogram.

B. Phantom

To obtain our original sinogram data, we used a tissue-equivalent anthropomorphic thorax phantom (Radiology Support Devices, Inc., Long Beach, CA) containing fillable cavities and organs to closely simulate an actual patient's geometry. All compartments were filled with known activity levels. The center of the heart chamber, the spine, and the lungs contained no activity, so it would be easier to evaluate the accuracy of the scatter distribution in these regions. The phantom was scanned using a Siemens/CTI 962 HR+ PET scanner with septa removed. Two-dimensional transmission scan data were processed to generate the transmission image and 3-D attenuation correction data. For simulation accuracy studies, we used data from a 45-min transmission scan. We used the known attenuation values of the phantom to reduce noise and increase accuracy in the transmission image; see Fig. 1(a). We also acquired a 200-million-count emission scan to reduce noise in the emission image; see Fig. 1(b).

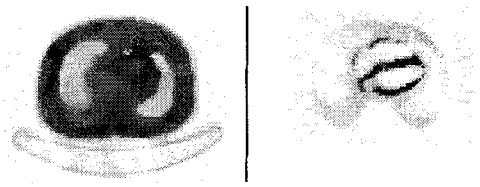

(a) (b)

Fig. 1. (a) A transaxial slice of the transmission image volume for the anthropomorphic phantom. (b) The corresponding emission image.

C. Techniques for Reducing Execution Time

The long execution time of most Monte Carlo 3-D PET simulations is a limiting factor in research applications and makes clinical scatter correction impractical. Therefore, most of our effort was spent optimizing the code for fast execution. In this section, we present techniques employed to reduce execution time and increase accuracy.

Our simulation utilizes an accurate photon transport method known as *delta scattering* [13]. Because photons do not have to be "stepped through" the attenuation medium, this method is fast and independent of matrix size; however, this technique is not compatible with certain variance reduction techniques such as forced detection and stratification [5].

We have developed stratification and variance reduction techniques that are compatible with our method of photon transport. The new "stratification" has two components. First, if the first photon of an annihilation pair is detected, the second simulated photon is split into multiple photons. Second, we implement a photon emission acceptance angle that depends on axial position. Information required to optimize these techniques for different objects is generated in a 30-s preprocessing phase that has been included in the total 4-min simulation time.

In Monte Carlo methods, a single photon can be divided into multiple photons, provided the resulting photons are weighted such that the sum of their weights is one. This method is known as *photon splitting* and will not bias the results of a simulation. If the first photon of an annihilation pair is detected, we simulate multiple second photons of equal weight. This is done so most single-photon detection events will result in at least one coincidence detection. The degree of second-photon splitting depends on axial position and emission angle. Less splitting is used for second photons that are more likely to result in detection. Using this method, accuracy is not affected, and the number of detected scatter coincidence events is increased by a factor of three to four for a given simulation time, depending on phantom geometry.

To implement the second-photon splitting technique without adding noise to the scatter distribution, it is important to consider two cases. When the first photon is detected without being scattered, the second photon is split at the point of annihilation.

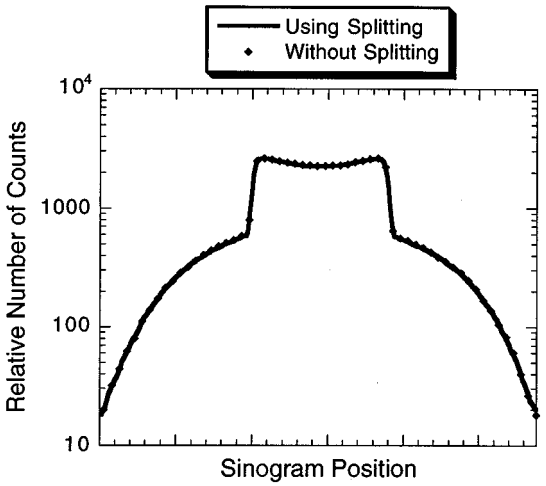

Fig. 2. Profiles of a single projection plane of simulated scatter with and without splitting the second photon. The mean standard deviation of the difference between these two curves is within the 0.7% noise level. To obtain this low level of noise in a single sinogram projection angle, the "splitting" simulation ran for 10 and the "nonsplitting" simulation ran for 34 h.

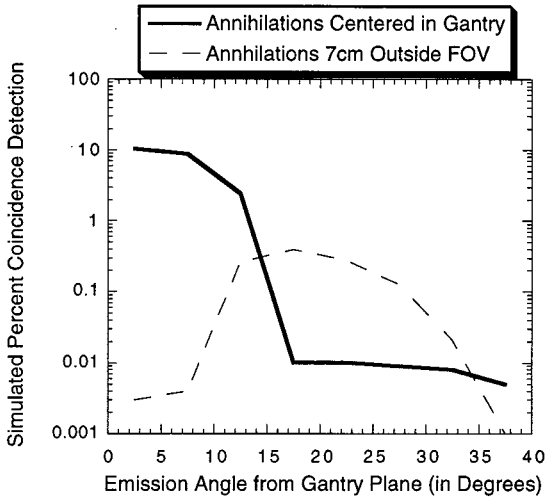

Fig. 3. Percent coincidence detection versus axial emission angle of annihilation photons for annihilations occurring inside and outside the FOV. Using the position-dependent acceptance angle, only annihilations with percent coincident detection above a threshold (— • —) are simulated. In this example, the centered annihilations emitting photons from 0° to 20° and the photons from outside the FOV emitted from 10° to 35° are simulated.

If, instead, it is determined that the first photon will undergo a scatter event, the second photon is simulated before the first photon's new scatter angle is calculated. If that second photon is detected, the first photon is split at the point of scatter. If that second photon is not detected, no coincidence can be recorded, and the next annihilation begins. To see if this method had any effect on simulation results, we compared simulation sinograms with and without using second-photon splitting. We saw no statistically significant difference between simulation sinograms for a noise level of 0.7% (see Fig. 2).

Most PET simulations use a stratification technique in which only photons emitted within a certain axial emission angle around the PET gantry are simulated. This saves computation time by not simulating annihilations that are unlikely to result in coincidence. By using an acceptance angle limit of 40° rather than 180° in our code, 4.6 times the number of coincidences are acquired for the same execution time; however, 4% of scatter events are lost. The resulting acquisition rate is 42 detected scatter coincidence events per millisecond. Using an acceptance angle of 70°, the acquisition rate is 35 scatter events per millisecond with only a 0.1% loss of scatter events. We have now implemented an acceptance angle that depends on axial position. The axial acceptance angle is narrow in the center of the field of view (FOV) but is wider, especially outside the FOV, to avoid losing a significant number of detectable scatter events. In addition, for some axial positions outside the FOV, it is inefficient to simulate photons that are emitted within 5° or 10° of parallel to the gantry plane (see Fig. 3). This is because it is unlikely for both annihilation photons to be scattered into the gantry so that a coincidence detection could occur. To determine optimal axial acceptance angles for different axial positions, the percent of annihilations resulting in coincidence detection as a function of axial emission angle of annihilation photons is determined during a brief presimulation. Then, for each position, only those angles with a coincidence detection rate above a given threshold are simulated. Using this technique, our simulation acquired 44 scatter coincidence events per millisecond with only a 0.3% loss.

For a nominal 350-keV energy threshold, there is actually a 23.8-keV deficit and an average 22.9% energy resolution FWHM spread on the ECAT HR+ [14]. This means the actual energy response of the scanner is the integral of a Gaussian centered at 326.2 keV with a 22.9% FWHM. To incorporate the true energy response of the scanner and reduce computation time, we force the first Compton interaction of each annihilation pair to result in a scattered photon that will be detected above the realistic energy threshold of the scanner. This is done by storing values that incorporate both the Klein–Nishina formula and the effect of the energy response of the system into a single array. This array determines scattered photon energy and corresponding scatter angle from random numbers. For multiple scatter events, the scattered photons are accepted or rejected based on their probability of acceptance above the energy threshold. This probability must take into account that the photon has already been accepted by the system's energy response in earlier scatter interactions.

This technique has many advantages. The calculation of scatter angle and energy for scattered photons together with the random acceptance or rejection of photon detection for a given energy are replaced by a single memory access, reducing computation. Simulation time is not wasted on photons that will be rejected due to the energy threshold of the system because they are rejected long before they reach the gantry. This also prevents loss of ~50% of the individual scattered photons in our simulation due to forcing and preserves the equal weighting of scatter coincidence events. This technique doubled the efficiency for simulating scatter events and increased its accuracy by incorporating the actual energy response of the scanner (see Fig. 4).

This technique is based on the principle that in Monte Carlo simulation, events do not need to be simulated in chronolog-

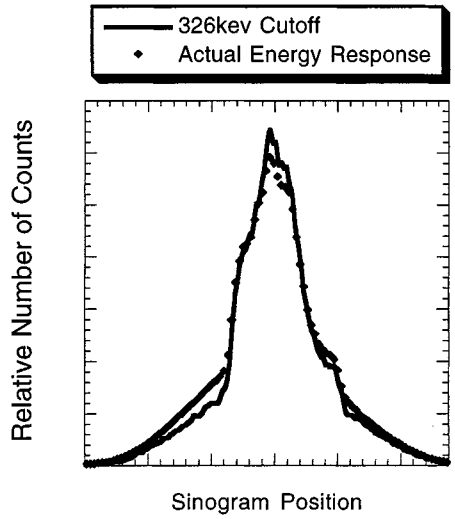

Fig. 4. Profiles (linear scale) of a projection plane of simulated totals (scatter + primary events) of the anthropomorphic phantom with and without considering the 22.9% energy resolution of the scanner. When the actual energy response of the scanner is modeled, the scatter distribution is broader and more accurately reflects measured results than when using a simple 326-keV cutoff.

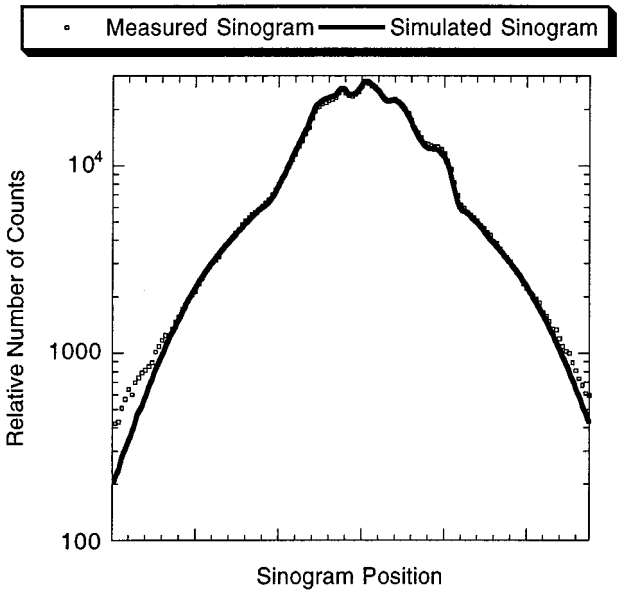

Fig. 5. A comparison of the simulated totals sinogram with the normalized sinogram measured from the scanner. The difference at the edge of the sinogram may be the result of greater acceptance of lower energy photons [14]. We plan to incorporate this deviation from Gaussian energy response by the scanner in the future.

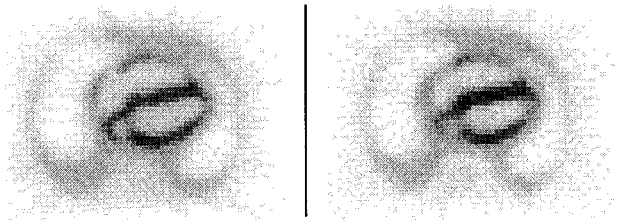

Fig. 6. A comparison of the measured and simulated total images. The left image is reconstructed without scatter correction from measured PET data, and the right image is simulated.

ical order. Events can be simulated in the order that results in the best efficiency, as long as probabilities are preserved. The method of taking into consideration the energy response of the detectors before photons reach the detectors can be applied to other modalities. It would be especially effective when modeling CT scanners or X-ray tubes that generate a polychromatic beam. By scaling the number of simulated photons for different energies by the energy response of the system prior to simulation, the noise in simulated data could be significantly reduced; however, this technique will corrupt the nature of the noise.

Our code currently acquires 44 000 scatter coincidences per second. At this simulation rate, many simulations generating data for investigation of scatter effects in PET can be performed in a day. The reduced computation time is also necessary for practical implementation of the Monte Carlo 3-D PET scatter correction in the clinic.

III. Results

A. Accuracy

For qualitative analysis of the accuracy of our simulation, we compared a projection of the normalized measured sinogram without scatter correction to a simulated total sinogram projection (see Fig. 5). For better quantitative analysis, we also compared reconstructed images from these sinograms. These images contain both the scatter and primary distributions, and, assuming perfect input data, theoretically they should be identical (see Fig. 6). The simulation sinograms were smoothed to the same degree as the measured sinograms prior to image reconstruction.

Quantitative analysis of the difference of these images is given in Table I. Region-of-interest (ROI) analysis was used to measure the level of scatter in five different regions in the thorax images.

We have seen evidence that the large error in the backbone region in this analysis is a result of setting the attenuation value of bone to that of tissue in our attenuation map processing. This is not a good approximation and will be corrected in future work. There is a statistically significant 5.5% underestimation of scatter in the ROI for the central heart chamber. The effect of the higher light output of edge crystals [14] is not yet incorporated in the model. We believe that this will result in greater acceptance of higher energy scattered photons and may be the reason for the 5.5% error in the center of the FOV. We found no significant error in any of the other ROIs for this study. We intend to perform a more rigorous analysis of accuracy on multiple phantoms.

TABLE I
A Comparison Between the Simulated Total Image and the Original PET Image Without Scatter Correction. Error Is Calculated Using the Standard Error (σ/#ofvoxels^2) of the ROI Volume

Mean ROI Values of Image Intensity		
Location of ROI	Monte Carlo Image of Primary + Scatter	Emission Image with no Scatter Correction
Heart Wall	4.59 ± 0.10	4.57 ± 0.12
Background	1.97 ± 0.03	1.96 ± 0.02
Center of Heart	1.03 ± 0.02	1.09 ± 0.03
Lung	0.24 ± 0.01	0.24 ± 0.02
Backbone	0.65 ± 0.02	1.01 ± 0.02

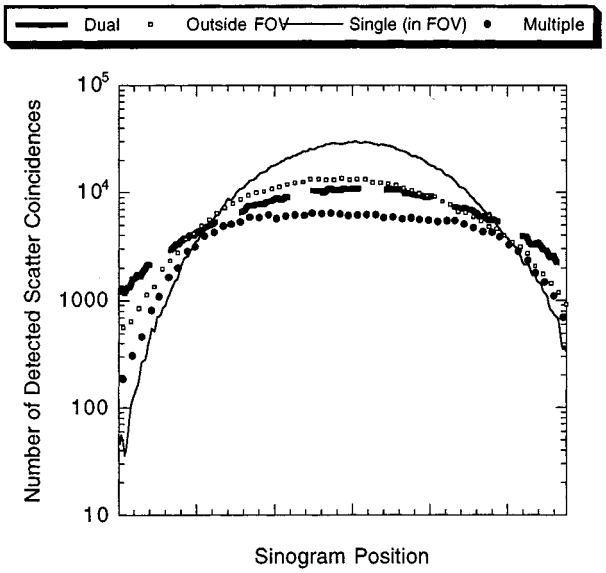

Fig. 7. Profiles of simulated sinograms of four different types of scatter. Each type of scatter has a shape distinct from other scatter types. The single scatter distribution is the narrowest.

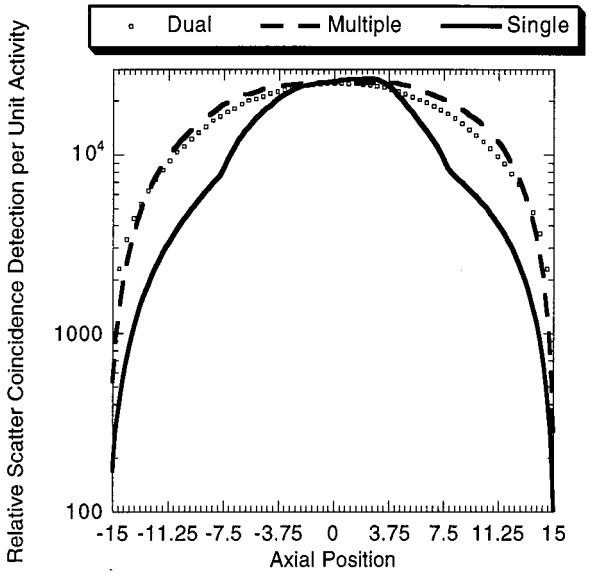

Fig. 8. This graph shows the original position (in centimeters from the center of the gantry) of annihilations that result in different types of scatter. Graphs have been scaled so that their shapes can be more easily compared. The fraction of multiple and dual scatter increases away from the center of the gantry.

B. Multiple Scatter and Out-of-FOV Scatter

Through Monte Carlo simulation of the anthropomorphic phantom, we found that 36.4% of the total scatter distribution were dual or multiple scatter events. These are especially difficult to calculate analytically. In fact, most scatter corrections ignore these effects [2], [12]. Of the scatter fraction, 22.0% were dual scatter events in which both detected photons had been scattered at least once. Of the scattered coincidences, 14.4% were multiple scatter events in which only one of the photons had been scattered more than once. Scatter from outside the FOV made up 27.5% of the total scatter distribution: 4.7% from multiple scatter events, 6.9% from dual scatter events, and 15.9% from single scatter. Although out-of-FOV scatter can be calculated analytically, most scatter corrections do not currently take it into account and only model single scatter from inside the FOV (accounting for 46.5% of the total scatter fraction for this study). These four different forms of scatter have different distributions, originate from different locations, and have a different dependence on initial emission angle; see Figs. 7–9.

All of these forms of scatter are automatically incorporated in the Monte Carlo method. Because of the different shape and origin of out-of-FOV, multiple, and dual scatter, each would have to be modeled individually in an analytical scatter correction that did incorporate these types of scatter.

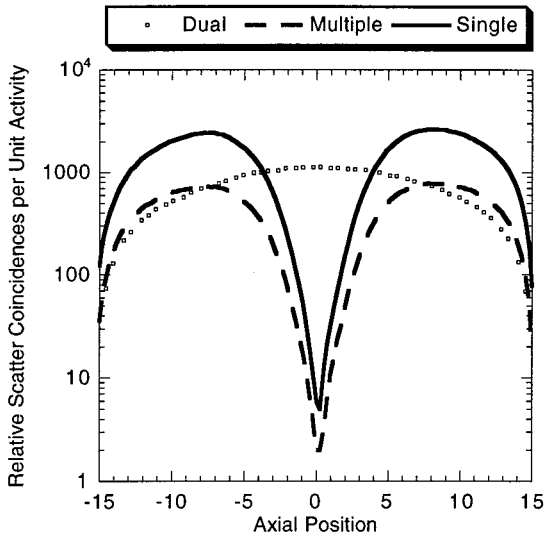

Fig. 9. This graph shows the original position (in centimeters from the center of the gantry) of annihilations that emit photons at an angle between 15° and 20° from parallel to the gantry and result in different types of scatter. The angular dependence of annihilation photons that result in multiple scatter events is similar to that for single scatter events. The shape of annihilation positions that result in dual scatter appears to have little angular dependence.

C. Scatter Correction

To apply the Monte Carlo scatter correction to 3-D PET studies, the emission sinogram must first be reconstructed to obtain the activity distribution (30 min on a 300-MHz Sun processor). We use the scatter correction method already on the system [12] for a best estimate of the input activity distribution. The transmission scan is processed in parallel to obtain the attenuation map (reconstructed in 2-D). The scatter sinogram is then calculated (currently in 4 min) using the Monte Carlo simulation. After subtracting the smoothed and scaled scatter estimate from the original normalized sinogram (1 min of smoothing), the resulting sinogram can be reconstructed to produce the final image. Thus, the current time cost of employing the Monte Carlo scatter correction is one extra 3-D reconstruction, 1 min of processing, and a 4-min simulation. By using exact FORE rebinning for the initial estimate [15], total image processing time could be reduced by almost a factor of two.

To analyze the potential effectiveness of the Monte Carlo 3-D PET scatter correction, we compared its performance with the analytical method currently used on Siemens scanners [12].

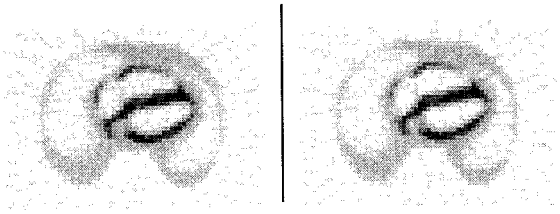

(a) (b)

Fig. 10. A comparison of (a) an image reconstructed using the analytical scatter correction with (b) an image reconstructed using Monte Carlo scatter correction. Although visually there are only subtle differences between the images, quantitatively the Monte Carlo corrected image is more accurate.

TABLE II
A COMPARISON OF SCATTER CORRECTED ROI VALUES WITH TRUE ACTIVITY CONCENTRATIONS. ACTIVITY VALUES ARE IN μCi/10 ml

Mean ROI Values of Activity Concentration			
Location of ROI	MC Scatter Correction	CTI's Scatter Correction	Activity in Phantom
Heart Wall	9.2 ± 0.6	9.5 ± 0.6	9.1 ± 0.2
Background	3.80 ± 0.12	4.07 ± 0.10	3.73 ± 0.04
Center of Heart	0.06 ± 0.10	0.64 ± 0.11	0
Lung	0.02 ± 0.08	0.14 ± 0.08	0
Backbone	-0.45 ± 0.06	-0.53 ± 0.06	0

Fig. 10 compares images reconstructed using the different scatter correction methods.

ROI values of five different regions in each image of Fig. 10 were compared with actual activity concentration levels in the phantom. Table II contains results of the quantitative analysis.

Concentration values in the ROIs for the heart wall have been corrected for partial volume and resolution effects. We had to be careful to avoid streak artifacts from filtered backprojection in ROIs drawn in the lung. In the future, we plan to use iterative reconstruction for better quantitative accuracy.

From Table II, we see that the image using the Monte Carlo scatter correction is more accurate than the scatter correction currently available on Siemens scanners for all regions. For this phantom study, there is a notable statistically significant difference in the central heart ROI where the scatter has been underestimated by six standard deviations using the analytical technique. There is no statistically significant difference between the Monte Carlo scatter-corrected and true activity concentrations for this study, except in the spine ROI where attenuation data were incorrect. There is evidence, however, that the 0.06 concentration in the central heart chamber ROI represents a real systematic error in the Monte Carlo scatter correction, even though it falls within the noise for this study. The effect of inaccuracy in the input images on scatter-correction performance is unclear. We intend to investigate how noise affects scatter-correction performance. We also plan to investigate alternatives to the global scale factor to reduce error when scaling the Monte Carlo simulated scatter sinogram to the measured sinogram.

IV. CONCLUSION

Our accelerated Monte Carlo simulation for an ECAT HR+ 3-D PET scan currently acquires 2.5 million detected scatter coincidence events per minute. This is ∼250 times faster than most other currently available Monte Carlo PET simulations [3]–[6] and ∼150 times faster than our original code [9], [10]. When comparing simulated and measured data for regions where input data were accurate, a 5.5% systematic error was observed in the center of the FOV for a low-noise phantom study. We believe this error is due to the greater acceptance of high-energy scatter events by block edge crystals. We intend to more rigorously investigate and improve upon the simulation's systematic accuracy and determine the effect of error in the input images on simulation results.

We have improved the accuracy and efficiency of our program. We have increased the sophistication of the stratification algorithm by simulating only annihilation photons emitted at angles that do not have a negligible contribution to simulated sinograms. In addition, we have introduced photon position and angle-dependent splitting of the second annihilation photon, which increased efficiency by over a factor of three. We also incorporated the actual energy response of the scanner while doubling computational efficiency.

We demonstrated that the Monte Carlo scatter correction for 3-D PET was more accurate than the scatter correction currently available on Siemens PET scanners for a low-noise phantom study. We intend to perform a more rigorous investigation of the effectiveness of the Monte Carlo 3-D PET scatter correction for different subject configurations over a range of noise levels. Eventually, we want to compare our scatter correction with various available scatter corrections, particularly with an analytical technique that does accurately model scatter from outside the FOV, which can account for ∼27.5% of the scatter fraction.

Small-animal 3-D PET scanners such as microPET are being used in research where quantitative analysis is performed. Scatter corrupts quantitative accuracy. Using Monte Carlo simulation, we have found that the scatter fraction in typical microPET studies ranges from 10% to 30% for subjects 2–8 cm in diameter. The amount of scatter is highly dependent on the axial extent of the subject. We want to use Monte Carlo simulation to analyze scatter in animal scanner imaging and eventually employ a Monte Carlo scatter correction on microPET data.

We are currently investigating methods of input data processing, particularly techniques to reduce noise in the attenuation map without compromising accuracy [16]–[18]. We will continue to use the Monte Carlo simulation to learn more about different types of scatter in microPET, 3-D brain studies, and whole-body PET. We also want to continue investigating the impact of scanner characteristics such as energy resolution, lead shields, and the patient bed on the resulting sinograms so that more can be understood when developing new scanners.

ACKNOWLEDGMENT

The authors would like to thank Dr. R. Harrison for discussions on variance-reduction techniques and Dr. C. Watson for information on detection response efficiency as a function of energy. The authors would also like to thank A. Goertzen, Dr. Y. Shao, and Dr. I. Chetty for sharing ideas concerning photon transport. They would also like to thank Dr. S. Cherry, Dr. A. Chatziioannou, and Dr. F. Beekman for theoretical discussions and D. McElroy, L. Pang, and R. Sumida for assistance with phantom scans.

REFERENCES

[1] S. R. Cherry, S. R. Meikle, and E. J. Hoffman, "Correction and characterization of scattered events in three dimensional PET using scanners with retractable septa," *J. Nucl. Med.*, vol. 34, p. 671, 1993.

[2] J. M. Ollinger and G. C. Johns, "Model-based scatter correction for fully 3D PET," *Phys. Med. Biol.*, vol. 41, pp. 153–176, 1996.

[3] I. Castiglioni, O. Cremonesi, M. C. Gilardi, V. Bettinardi, G. Rizzo, A. Savi, E. Bellotti, and F. Fazio, "Scatter correction techniques in 3D PET: a Monte Carlo evaluation," *IEEE Trans. Nucl. Sci.*, vol. 46, pp. 2053–2058, Dec. 1999.

[4] C. J. Thompson, J. M. Cantu, and Y. Piccard, "PETSIM: Monte Carlo program simulation of all sensitivity and resolution parameters of cylindrical positron imaging systems," *Phys. Med. Biol.*, vol. 37, pp. 731–749, 1992.

[5] D. R. Haynor and R. L. Harrison *et al.*, "Improving the efficiency of emission tomography simulations using variance reduction techniques," *IEEE Trans. Nucl. Sci.*, vol. 37, pp. 749–753, Apr. 1990.

[6] H. Zaidi, A. Scheurer, and C. Moral, "An object-oriented Monte Carlo simulator for 3D positron tomographs," *Comput. Meth. Programs Biomed.*, vol. 58, pp. 133–145, 1999.

[7] I. Castiglioni, private communication, June 2000.

[8] H. Zaidi, "Relevance of accurate Monte Carlo modeling in nuclear medical imaging," *Med. Phys.*, vol. 26, pp. 574–608, April 1999.

[9] C. S. Levin, Y. Tai, M. Dahlbom, T. H. Farquhar, and E. J. Hoffman, "Removal of the effect of Compton scattering in 3D whole body PET by Monte Carlo," in *1995 Nuclear Science Symp. Medical Imaging Conf. Rec.*, vol. 2, Oct. 1995, pp. 1050–1054.

[10] C. S. Levin, M. Dahlbom, and E. J. Hoffman, "A Monte Carlo correction for the effect of Compton scattering in 3D PET brain imaging," *IEEE Trans. Nucl. Sci.*, vol. 42, pp. 1181–1185, Aug. 1995.

[11] C. H. Holdsworth, C. S. Levin, M. Janecek, M. Dahlbom, and E. J. Hoffman, "Investigation of accelerated Monte Carlo techniques of PET simulation and 3D PET scatter correction," *IEEE Trans. Nucl. Sci.*, vol. 48, pp. 74–81, Feb. 2001.

[12] C. C. Watson *et al.*, "Evaluation of simulation-based scatter correction of 3D cardiac imaging," *IEEE Trans. Nucl. Sci.*, vol. 44, pp. 90–97, Feb. 1997.

[13] E. R. Woodcock *et al.*, "Techniques used in the GEM code for Monte Carlo neutronics calculation," in *Proc. Conf. Applications of Computing Methods to Reactors*, 1965, ANL-7050, p. 557.

[14] C. C. Watson, "A technique for measuring the energy response of a PET tomograph using a compact scattering source," *IEEE Trans. Nucl. Sci.*, vol. 44, pp. 2500–2508, Dec. 1997.

[15] M. Defrise, P. E. Kinahan, D. W. Townsend, C. Michel, M. Sibomana, and D. F. Newport, "Exact and approximate rebinning algorithms for 3-D PET data," *IEEE Trans. Med. Imag.*, vol. 16, pp. 145–158, 1997.

[16] F. J. Beekman, E. T. P. Slijpen, and W. J. Niessen, "Selection of task-dependent diffusion filters for the post-processing of SPECT images," *Phys. Med. Biol.*, vol. 43, pp. 1713–1730, 1998.

[17] K. Kitamura, H. Iida, M. Shidahara, S. Miura, and I. Kanno, "Noise reduction in PET attenuation correction using nonlinear Gaussian filters," *IEEE Trans. Nucl. Sci.*, vol. 47, pp. 994–999, June 2000.

[18] C. Riddell, P. Brigger, R. E. Carson, and S. L. Bacharach, "The watershed algorithm: A method to segment noisy PET transmission images," *IEEE Trans. Nucl. Sci.*, vol. 46, pp. 713–719, June 1999.